Materials Today Bio 13 (2022) 100183

Contents lists available at ScienceDirect

Materials Today Bio

journal homepage: www.journals.elsevier.com/materials-today-bio

Thermogels containing sulfated hyaluronan as novel topical therapeutics for treatment of ocular surface inflammation

Duc Dung Nguyen [a,1], Li-Jyuan Luo [a,1], Jui-Yang Lai [a,b,c,d,*]

[a] Graduate Institute of Biomedical Engineering, Chang Gung University, Taoyuan, 33302, Taiwan
[b] Department of Ophthalmology, Chang Gung Memorial Hospital, Linkou, Taoyuan, 33305, Taiwan
[c] Department of Materials Engineering, Ming Chi University of Technology, New Taipei City, 24301, Taiwan
[d] Research Center for Chinese Herbal Medicine, College of Human Ecology, Chang Gung University of Science and Technology, Taoyuan, 33303, Taiwan

ARTICLE INFO

Keywords:
Sulfated hyaluronic acid
Thermogel
Leukocyte infiltration
Tissue protection
Ocular surface inflammation

ABSTRACT

The development of long lasting therapeutic agents is critically important for efficient treatment of chronic diseases. We herein report a rational strategy to develop a therapeutic thermogel featured with prolonged anti-inflammatory and corneal-protective effects. Specifically, a hyaluronic acid with different sulfation degrees and an amine-terminated poly(*N*-isopropylacrylamide) are conjugated to achieve the thermogels. *In vitro* studies reveal that the thermogels are highly biocompatible to statens seruminstitut rabbit cornea cells and their anti-inflammatory properties are strongly dependent on the sulfation degree. In a rabbit model of ocular inflammation, single-dose topical administration of a thermogel formulation could repair defects in corneal epithelium (~99% thickness restored), prevent corneal cell apoptosis (~68.3% cells recovered), and suppress ocular surface inflammation (~4-fold decrease) for a follow-up period of 7 days. This high treatment efficacy of the thermogel can be attributed to its potent inhibition in selectin-mediated leukocyte infiltration as well as effective corneal protection. These findings show a great promise for topical treatment of ocular inflammation and advancement of ophthalmic formulations using the bioactive thermogel as a therapeutic component that is not rapidly cleared from the eye and thus considerably reduces administration times.

1. Introduction

With the rapid growth of electronic display-related visually demanding tasks and the steady increase of aged population in the modern world, there is a cumulative trend of people living with ocular surface disorders such as dry eye disease (DED) [1–4]. DED is globally prevalent with up to 35% of the world population and imposes substantial economic burdens (e.g., ~$55 billion spent for annual societal costs in the United States) [5]. Typical symptoms of DED are blurry vision, irritation, light sensitivity, and ocular pain, all of which hinder daily activities, induce damage to the eye, and thus reduce quality of life [6,7]. Although the pathogenesis of DED has not been well documented, there is growing evidence that links DED with ocular surface inflammation [8]. The first-line treatment of DED is topical administration of artificial tears, eye drops, or their combination that serve to increase water retention and suppress inflammation on the ocular surface, accordingly reducing discomfort and alleviating pain in the unhealthy eye [9,10]. However, this gold standard intervention only can provide short-term relief due to rapid clearance of solution formulations triggered by tear dilution and the lacrimal drainage system [11]. To overcome this issue, frequent administration is required to mitigate the persistent ocular disease. Nevertheless, the highly repetitive administration supplies large cumulative doses to the eye, consequently causing high risks of adverse effects such as burning, stinging, and foreign object sensation [12]. Therefore, it is highly desired to develop alternative therapies for effectively attenuating the ocular surface inflammation while considerably reducing administration times.

Inflammation is pervasive in DED and considered the primary target in clinical assessment and treatment. It has been reported that the ocular inflammation in DED is pathophysiologically mediated by continuing activation and infiltration of pathogenic leukocytes in the conjunctiva and cornea [13,14]. Immuno-histopathological studies have indicated that patients with both Sjögren's syndrome and non-Sjögren's syndrome-related DED revealed similar conjunctival inflammation, as

* Corresponding author. Graduate Institute of Biomedical Engineering, Chang Gung University, Taoyuan, 33302, Taiwan.
E-mail address: jylai@mail.cgu.edu.tw (J.-Y. Lai).
[1] Equal contribution to first author.

https://doi.org/10.1016/j.mtbio.2021.100183
Received 12 November 2021; Accepted 2 December 2021
Available online 3 December 2021

verified by T cell infiltration, T cell upregulation, and elevated expression of lymphocyte activation markers [15]. Moreover, the numbers of infiltrated leukocytes and intracellular adhesion molecules in ocular tissues of both human patients and experimental animals afflicted with DED were found to increase with the increasing levels of inflammatory cytokines (e.g., interleukin (IL)-6, monocyte chemotactic protein (MCP)-1, or tumor necrosis factor alpha (TNF-α)) in the tear film and ocular epithelium [16–22]. In this regard, anti-inflammatory agents such as corticosteroids have been employed to suppress the elevated concentrations of cytokines in the chronic ocular disease [23]. Nevertheless, the repeated administration of corticosteroids could be implicated in more severe conditions such as glaucoma and retinopathy [24,25]. Accordingly, addressing the underlying inflammation mediated by infiltration of leukocytes into ocular surface tissues (e.g., selectin-mediated leukocyte recruitment [26] would be greatly beneficial to the treatment of DED with minimal side effects.

Hyaluronic acid (HA) is an anti-inflammatory polysaccharide that is widely distributed in connective, neural, and epithelial tissues as well as in ocular fluids [27]. Because of its strong dehydration resistance, good biocompatibility, and potent anti-inflammatory activity, HA has been demonstrated as a therapeutic polymer for protecting corneal epithelial cells and ocular surface as well as stabilizing tear film in DED [27–30]. Considering that selectins, a family of cell adhesion molecules, play an essential role in early stage of leukocyte recruitment-mediated inflammation [26], adding selectin-binding function to HA is an effective approach to enhance anti-inflammatory properties of the polysaccharide while maintaining its capability of protecting ocular surface tissues and stabilizing the tear film. In this context, chemical sulfation is a potent means of binding HA with selectin via electrostatic interaction between sulfate groups and basic amino acid residues of the protein. For example, sulfated HA (sHA) has been demonstrated to be able of blocking the selectin-dependent infiltration of leukocytes in acute lung injury and glomerulonephritis [31–33]. The inhibitory effects of sHA can be ascribed to the strong binding affinity between the sulfated polysaccharides and selectin, which interferes/competes with selectin binding to the native ligands on the tissues (i.e., reducing leukocyte infiltration into the tissues and thereby suppressing inflammation) [31]. Very recently, sHA has been covalently functionalized with collagen fibrils to form a stable scaffold, which could reduce the proinflammatory macrophage M1 response without inducing multinucleated giant cell formation during 30 days [34]. These results suggest a promising biomaterial that can modulate the inflammatory response for full-thickness skin regeneration. It is noting that the degree of sulfation in sHA is a key factor in determining binding affinities of the modified polysaccharides and their combined forms [35]. Inspired by these earlier findings and considering that DED is the chronic disease requiring long-term treatments, we hypothesize that a rational design of sHA with an ocular surface temperature-induced gelling material can be critically important for extending sHA residence on the ocular surface, accordingly formulating a new ophthalmic therapeutic with potent anti-inflammatory activity and prolonged corneal protection.

In this study, we present an ocular surface-responsive strategy for developing a long-acting therapeutic agent via an EDC/NHS coupling chemistry of sHA with amine-terminated poly(*N*-isopropylacrylamide) (PN-NH_2). The rational design to obtain the sHAPN therapeutic agent is based on sHA with different sulfation degrees, which are achieved by nucleophilic substitution of hydroxyl hydrogens on HA backbone chains with sulfur trioxide (SO_3) from its complexes containing *N,N*-dimethylformamide and pyridine, respectively. As expected, the resultant sHAPN copolymer possesses temperature-induced phase change characteristics, showing the lower critical solution temperature (LCST) of less than 30 °C [36]. The sHAPN copolymer can be transformed into gel upon contacting with the ocular surface, thereby increasing its resistance to the clearance action of the eye. In a rabbit model of DED, single-dose topical instillation of the sHAPN copolymer can effectively repair corneal epithelial defects, prevent cell apoptosis, and suppress ocular surface inflammation for a follow-up period of 7 days, possibly via sustaining the inhibitory effects on selectin-mediated leukocyte infiltration and extending the corneal-protective activities of the sHA. The findings suggest an efficient therapeutic agent for topically treating DED and harnessing the bioactive thermogel as an elongated, intrinsic therapeutic component for various ophthalmic formulations toward efficient management of complex ocular diseases.

2. Experimental

2.1. Materials

Hyaluronic acid sodium salt with weight-average molecular weight of ~1100 kDa was supplied from Kewpie (Tokyo, Japan) in a form of dry powder. 1-ethyl-3-(3-dimethyl aminopropyl) carbodiimide hydrochloride (EDC), *N,N*-dimethylformamide (DMF), sulfur trioxide-DMF complex, and sulfur trioxide pyridine complex were purchased from Sigma-Aldrich (St. Louis, MO, USA). *N*-hydroxysuccinimide (NHS) and *N*-isopropylacrylamide (NIPAAm) were supplied by Acros Organics (Geel, Belgium). Before use, NIPAAm was purified by recrystallization from *n*-hexane. 2,2′-azobisisobutyronitrile (AIBN) was obtained from Otsuka Chemical (Tokyo, Japan). 2-aminoethanethiol hydrochloride (AESH) was purchased from Tokyo Chemical Industry (Tokyo, Japan). Phosphate-buffered saline (PBS, pH 7.4) was obtained from Biochrom (Berlin, Germany). Eagle's Minimum Essential Medium (MEM) was provided by Gibco-BRL (Grand Island, NY, USA). Fetal bovine serum (FBS) was acquired from Biological Industries (Kibbutz Beit Haemek, Israel). All the other chemicals were of reagent grade and used as received.

2.2. Synthesis of sHA and PN-NH_2

In a typical experiment for the synthesis of sHA, 2 g of HA was dissolved in 400 mL of deionized water followed by an addition of 20 g of tetrabutylammonium (TBA). The resultant solution was stirred overnight, then filtrated, lyophilized, and dried at 35 °C under vacuum conditions. For the preparation of sHA with low sulfation degree (lsHA), 2 g of the as-prepared HA TBA salt was dispersed in 400 mL of DMF under Ar flow at room temperature. To this dispersion, 3.6 g of SO_3-pyridine complex in DMF (40 mL) was added, and the reaction solution was stirred for 20 min. In another experiment for the preparation of sHA with high sulfation degree (hsHA), 400 mL of HA TBA salt (2 g) in DMF was mixed with 40 mL of SO_3-DMF (9.9 g) in DMF, and the mixed solution was stirred for 1 h at room temperature [35]. To the reaction mixtures, acetone (2.8 L) was added to precipitate the sHA products, which were then filtered through a 0.45 μm membrane filter (Millipore) and neutralized with ethanolic sodium hydroxide solution. The resultant products were washed with excess acetone, dialyzed against deionized water, lyophilized, and dried under vacuum conditions to obtain sHA with different sulfation degrees.

In the experiment for preparation of the PN-NH_2, NIPAAm monomers were polymerized using AIBN as an initiator and AESH as a chain transfer agent. In short, 5 g of NIPAAm was dissolved in 10 mL of DMF with 0.21 g of AESH. The solution was then bubbled with dry nitrogen for 30 min, followed by an addition of 0.1 g of AIBN [37]. The polymerization process was performed at 70 °C for 6 h under a vacuum condition. Next, the reactant was precipitated into excess diethyl ether and dried at room temperature under a low pressure atmosphere. The dried product was purified by iterative precipitation and dissolution in hot water before lyophilization.

2.3. Synthesis of sHAPN thermogels

To obtain the sHAPN copolymers, sHA and PN-NH_2 were dissolved in deionized water to a concentration of 0.5 wt% (the weight ratio of sHA/PN-NH_2 is 3:7). To this solution, EDC and NHS were added to facilitate the formation of amide bonds between the sodium carboxylate groups of

hyaluronic acid and the amino groups of PN-NH_2. The sHA/EDC/NHS molar ratio in the mixture is 2:2:1 with a reference to the sodium carboxylate group of hyaluronic acid. The mixture was then continuously stirred overnight at room temperature followed by a precipitation in a tetrahydrofuran-hexane solution (4:1). Finally, the precipitant was purified by Soxhlet extraction with methanol, dialyzed against deionized water for 3 days, and then lyophilized to achieve the sHAPN thermogels.

2.4. Structure and property characterization of materials and thermogels

The formation of functional groups and characteristic peaks of sHA, PN-NH_2, and sHAPN specimens were probed using proton and carbon nuclear magnetic resonance ($^1H/^{13}C$ NMR) and Fourier transform infrared (FTIR) spectroscopies. The NMR measurements were performed using a Bruker Avance DRX 500 NMR. The FTIR spectra were recorded in the range of 4000–400 cm^{-1} with a resolution of 8 cm^{-1} utilizing a FTIR spectrophotometer (FT-730 Horiba, Japan). Elemental composition was analyzed using energy dispersive X-ray spectroscopic microanalysis (6560 INCA, Oxford Instruments, Concord, MA, USA). Doppler microelectrophoresis (Zetasizer Nano ZS, Malvern Instruments, Worcestershire, UK) was employed for zeta potential measurement ($n = 5$). Molecular weights (Mws) were determined via gel permeation chromatography measurement using a system consisted of a HPLC-pump and a RI 2000 refractive index detector (Schambeck SFD) with four columns (Shodex SB series, Showa Denko): OHpak SB-802 HQ (exclusion limit 4 $\times 10^3$ Da), OHpak SB-802.5 HQ (exclusion limit 1 $\times 10^4$ Da), OHpak SB-803 HQ (exclusion limit 1 $\times 10^5$ Da), and OHpak SB-804 HQ (exclusion limit 1 $\times 10^6$ Da). The mobile phase was PBS buffer, and the flow rate was 0.5 mL/min. For size calibration to determine Mws of sHA, pullulan standards were utilized [35]. The graft yield was calculated as follow: Graft yield (wt%) = [(Wf - Wi)/Wi] $\times$ 100], where Wi and Wf respectively are the weight of sHA or HA before grafting and the total weight after the PN-NH_2 reacting with sHA or HA backbone chain. Turbidity characteristic was carried out by quantifying change in optical absorbance in response to temperature via a UV–Vis spectrophotometer (Thermo Scientific, Waltham, MA, USA). To this end, polymeric samples were dissolved in artificial tear solution (ATS) to a concentration of 10% (w/v) and then incubated at 25 °C for 1 h prior to being positioned in a thermostatic cell holder programmed at 32 °C. At pre-determined time intervals, optical absorbance (at 470 nm) of the polymeric solutions was recorded. The gel formation time (GFT) was the time at which the optical absorbance was at the half between the highest and lowest values ($n = 5$). A differential scanning calorimeter (DSC, TA Instruments, New Castle, DE, USA) was utilized for measurement of the lower critical solution temperature (LCST) of the polymeric samples. At first, the polymeric samples were dissolved in the ATS, which is composed of 124 mM Na^+, 133 mM Cl^-, 24 mM HCO^{3-}, 30 mM K^+, 0.7 mM Mg^{2+}, 0.7 mM Ca^{2+}, 0.35 mM glucose, 4.5 mM urea, 3.5 mM lactate, and 0.2 mM pyruvate, to a concentration of 10% (w/v). Then, the solutions were hermetically sealed in aluminum pans. To obtain DSC data, the samples were heated from 23 to 35 °C at a ramp rate of 3 °C/min. LCSTs were defined as the onset point of the endothermic peaks in the DSC patterns ($n = 5$). Rheological characterization was performed using an AR2000ex rheometer (TA Instruments) with a Peltier controller and a parallel plate geometry (diameter of 25 mm). Before each measurement was commenced, the inertia of the instrument was calibrated. The developed copolymers were dissolved in the ATS at 10% (w/v). Storage (G') and loss (G") moduli of the copolymer solutions were recorded in response to temperature changes. The solutions were heated from 20 to 40 °C at a rate of 1 °C/min while subjecting to a 5% oscillatory strain at 1 Hz; measurements were evaluated in the viscoelastic linear region. To evaluate the degradability of different polymeric samples, their weight remaining was measured. Degradation tests were performed in a water bath at 32 °C for 10 min using the polymeric solutions at the concentration of 10% (w/v). The initial dry weight (W_i) of polymeric sample was measured when it was in a steady weight. Next, the dry polymeric sample was immersed in an ATS containing 100 U/mL of hyaluronidase at 32 °C [38]. At predetermined time intervals, the degraded gelling material was collected, washed with deionized water, and dried in vacuum to reach a steady dry weight (W_d). The percentage of weight remaining (%) was calculated as follow: (W_d/W_i) $\times$ 100 ($n = 5$).

2.5. Biocompatibility studies

Statens Seruminstitut rabbit cornea (SIRC) cells (BCRC no. 60093), purchased from the Bioresource Collection and Research Center (Hsinchu, Taiwan, ROC), were grown in a culture medium (Eagle's Minimum Essential Medium) supplemented with 10% fetal bovine serum (FBS) and 2% non-essential amino acids. The cell cultures were incubated at 37 °C in a humidified atmosphere containing 5% CO_2. The medium was replaced two times per week. SIRC cells were subcultured by trypsinization at a split ratio of 1:3. Next, the SIRC cells (5×10^4 cells/well) were seeded into 24-well plates by 1 mL/well. Each well of the 24-well plate was separated into two parts via cell culture inserts (Falcon 3095, Becton Dickinson Labware, Franklin Lakes, NJ, USA). The medium was then substituted by a fresh culture medium that contains different polymeric samples. The temperature-triggered in situ gel method (as aforementioned) was employed to prepare gelling polymeric samples, followed by adding them to the inner part of the double-chamber system. The cultured cells grown without any test materials worked as a control (Ctrl) group. The SIRC morphology was characterized by a phase-contrast microscope (Nikon, Melville, NY, USA) after the cell cultures exposed to different polymeric samples for 2 days. Moreover, a cell proliferation mitochondrial dehydrogenase (MTS) assay was utilized to assess the cell metabolic activity. The optical absorbance was measured at 490 nm using a microplate spectrophotometer, and the results were expressed as relative MTS activities compared to that of the Ctrl ($n = 6$). In addition, cell viability of the cultures exposed to different polymeric samples for 2 days was assessed using a live/dead assay. Specifically, the exposed cell cultures were washed with PBS three times and stained with the live/dead viability/cytotoxicity kit comprising calcein acetoxymethyl and ethidium homodimer-1 to detect the live and dead cells, respectively. A fluorescence microscope (Carl Zeiss, Oberkochen, Germany) was employed to count the number of live and dead cells. The cell viability was expressed as the average ratio of live cells to the total number of cells ($n = 6$).

2.6. Anti-inflammatory activity studies

Anti-inflammatory activities of the polymeric samples were evaluated by enzyme-linked immunosorbent assays (ELISA). To this end, SIRC cells (5×10^4 cells/well) were seeded in 24-well plates containing regular growth medium and then incubated overnight. To induce inflammation, interleukin-1β (IL-1β) stimulation was employed by replacing the medium with the fresh one containing 1 ng/mL of IL-1β. Different gelling samples were respectively added to the inner well of the double-chamber system at 37 °C to examine their anti-inflammatory activities on the IL-1β-stimulated cell cultures. Untreated and IL-1β-stimulated SIRC cells incubated with no test material served as the negative control (NC) and positive control (PC) groups, respectively. After a 3-day incubation, the levels of IL-6, MCP-1, and TNF-α released from untreated/treated SIRC cells were measured by the ELISA kits according to the manufacture instructions ($n = 6$). Inhibitory effects of the polymeric samples on the selectin was evaluated via the binding activity of the soluble fusion protein of rat L-selectin and human IgG (LEC-IgG) to sulfatide [32]. First, sulfatide at a concentration of 1.6 μg/mL in PBS was prepared and applied to 24-well plates and then allowed to be stable. Subsequently, the plates were blocked in blocking buffer (1% bovine serum albumin (BSA)/PBS) at room temperature for overnight. After that, fat was removed from BSA by a solution of chloroform and methanol (2:1). Diluted polymeric samples (30 μg/mL) were preincubated with 1.6 μg/mL LEC-IgG in 0.1% BSA-20 mM Tris buffer (pH 7.4) comprising 1

mM Ca^{2+} and Mg^{2+} at room temperature for 30 min. Next, the plates were washed 6 times with PBS and incubated with 50 μL of the pre-incubated solution at room temperature for 120 min. To the plates, 50 μL of (1000-fold dilution) HRP-conjugated anti-human IgG/IgM/IgA antibody was added and incubated for 90 min at room temperature. The color reaction was carried out by incubating the plates (after washing 10 times) with O-phenylenediamine (Sigma Aldrich) in 50 μL of citrate buffer (pH 5.6) containing 2 μL of 30% hydrogen peroxide. Binding activity was quantified with a microplate reader at 490 nm with a reference correction at 630 nm.

2.7. Therapeutic treatment studies

Twenty-four female adult New Zealand white rabbits (National Laboratory Animal Breeding and Research Center, Taipei, Taiwan, ROC) were employed to study therapeutic effects of the sHAPN thermogels. All the animal eyes were healthy and showed no observable abnormalities. At the time of the DED induction test, the rabbits were 20 weeks old and weight of 3.2 ± 0.25 kg. Procedures for animal studies were approved by the Institutional Animal Care and Use Committee of Chang Gung University (Approval Number: CGU109-031) and were carried out according to the ARVO Statement for the Use of Animals in Ophthalmic and Vision Research. Topical administration of 0.1% benzalkonium chloride was applied twice daily on the animal eyes for 14 days to create dry eye disease in the test rabbits [39]. Specifically, the rabbits were categorized into six groups including Pre (healthy eyes, n = 24), DED (as-induced dry eyes, n = 24), Ctrl (dry eyes treated with 50 μL ATS, n = 6), HAPN (dry eyes treated with HAPN, n = 6), lsHAPN (dry eyes treated with lsHAPN, n = 6), and hsHAPN (dry eyes treated with hsHAPN, n = 6). Polymeric formulations were prepared by dissolving the polymer specimens in ATS at a 10% w/v concentration, followed by filtration through a 0.22 μm Millipore filter membrane. For therapeutic treatment studies, 50 μL of each polymeric formulation (single dose) was instilled onto the lower conjunctival sac of the rabbit eyes. Treatment efficacy of the formulations was assessed for a follow-up period of 7 days. The animals were first anesthetized intramuscularly with 2.5 mg/kg body weight of tiletamine hydrochloride/zolazepam hydrochloride mixture (Zoletil; Virbac, Carros, France) and 1 mg/kg body weight of xylazine hydrochloride (Rompun; Bayer, Leverkusen, Germany). Corneal fluorescein and rose bengal staining examination were then conducted for observations, respectively. The stained ocular surfaces were inspected and graded by slit-lamp biomicroscopy (Topcon Optical, Tokyo, Japan) after topically instilling 1% fluorescein sodium/rose bengal (2 μL) into the conjunctival sacs. For the animal eyes tested with fluorescein stain, the fluorescence intensity was measured on the cornea under cobalt blue light on a slit-lamp biomicroscope. The level of rose bengal staining in both conjunctiva and cornea was also quantitatively analyzed. A regular four-point scale (0 = none, 1 = mild, 2 = moderate, and 3 = severe) was used in each of three regions for data analysis [40]. The staining scores were in the range of 0–9 (n = 6). Tear production was assessed by Schirmer test. Each Schirmer paper strip (Color Bar Schirmer Tear Test, EagleVision, Memphis, TN, USA) was placed into the lower eyelid pouch without anesthesia. The wetted length of the strip was measured after 3 min being kept in the eyelid pouch (n = 6) [41]. For histology and morphology examinations, the test rabbits were euthanized with carbonic dioxide at the end of the follow-up (i.e., day 7 post-administration). In particular, rabbit corneas were histologically examined. After excised from the experimental eyes, the corneal tissues were fixed in 4% paraformaldehyde in phosphate-buffered saline, dehydrated in a graded series of ethanol solutions, embedded in paraffin, and cut into 5 μm sections. Next, these sections were stained with hematoxylin and eosin (H&E) and checked under a light microscope (Carl Zeiss) for the thickness measurement of the corneal epitheliums. In another histological analysis of the tissue sections, terminal deoxynucleotidyl transferase (TdT)-mediated dUTP nick end labeling (TUNEL) assay (Roche Diagnostics) was used to evaluate the apoptosis of corneal epithelial cells. Specifically, the tissues were fixed with 4% paraformaldehyde, then permeabilized in 0.1% Triton X-100 in 0.1% sodium citrate for 2 min on ice, and incubated with a mixture of TdT solution and fluorescein isothiocyanate dUTP solution in a humidified chamber at 37 °C for 1 h. The negative controls were incubated with deionized water instead of TdT enzyme. Subsequently, the tissue sections were counterstained with 4', 6-diamidino-2-phenylindole (DAPI; Vector, Peterborough, England) and visualized under fluorescence microscope (Carl Zeiss) for cell nuclei imaging. Three regions were randomly selected, and the number of TUNEL-positive apoptotic cell nuclei was quantitatively analyzed. For microscopic analysis of microvilli structural morphology, the corneal tissues were fixed in 2.5% glutaraldehyde in 0.1 M phosphate buffer (pH 7.4) at 4 °C for 24 h. Then, the specimens were post-fixed with 1% osmium tetroxide in 0.1 M phosphate buffer for 2 h and dehydrated in a graded series of ethanol at 4 °C. Finally, the dehydrated specimens were dried, coated with gold, and examined by a scanning electron microscope (JSM-7500 F, JEOL, Tokyo, Japan).

2.8. Statistical analyses

Results were expressed as mean ± standard deviation (SD). Significance was evaluated by one-way analysis of variance (ANOVA) and accepted with $P < 0.05$.

3. Results and discussion

Our approach to formulate the therapeutic thermogels is based on the manipulation of sulfation degrees in the sHA through the replacement of hydroxyl hydrogens with sulfur trioxide, radical polymerization of thermo-responsive PN terminated with amine groups, and formation of amide linkage between the sHA and PN-NH_2 (Fig. S1). To confirm the presence of amine groups at the end chain of the PN, ^{1}H NMR and FTIR spectroscopies were employed. Fig. 1a shows ^{1}H NMR spectra of PN-NH_2 and NIPAAm in D_2O; inclusion of NIPAAm pattern is aimed for comparison. The chemical shift around 1.1 ppm can be ascribed to the presence of methyl groups [42]. The peak at 3.9 ppm is characterized for –NH-CH– while those in the range of 5.6–6.2 ppm are possibly due to vinyl proton [43]. The broad signals from 1.3 to 2.1 ppm also imply the presence of amine groups for the methylene proton rather than vinyl proton peaks in the NIPAAm specimen. In addition, the presence of new peaks at 2.7 and 2.9 ppm signifies the presence of NH_2 and the introduction of the chain-transfer agent to the PN [44]. FTIR spectra (Fig. 1b) further support the formation of PN-NH_2, as verified by (i) the visibility of amide bands I and II at 1657 and 1546 cm^{-1}, (ii) the disappearance of monomer characteristic peaks at 1617 cm^{-1} (C═C) and 1411 cm^{-1} (=CH_2), and (iii) the occurrence of primary amine (NH_2) peak at 3438 cm^{-1} [45,46]. The sulfation degree in the sHA specimens were characterized using carbon-13 NMR (^{13}C NMR), as shown in Fig. 1c. Compared to the ^{13}C NMR spectrum of the HA, there is an obvious change in the C-6 peak position of the primary CH_2- group in the N-acetyl-glucosamine unit, displaying a downfield shift from 61 ppm to 68 ppm in both sulfated samples.

These results suggest that the OH group at C-6 position in the HA was mostly sulfated by the two SO_3 complexes [47]. Other carbon peaks (C-4, C-2′, and C-3′) revealed differently with respect to the sulfation reactions. Specifically, the sHA with low sulfation degree (lsHA) exhibited similar carbon signals without any chemical shifts as compared to the unsulfated HA, while a full attribution of the carbon peaks was relatively complicated for the high sulfation sample (hsHA). In addition to the complete sulfation at C-6 position, the ^{13}C NMR spectra also imply the diverse possibilities of sulfation degrees on the OH groups of the HA, indicating those at C-4 position were sulfated at a greater extent compared to C-2′ and C-3' [48]. Additionally, FTIR spectra (Fig. 1d) of HA, lsHA, and hsHA were also recorded to qualitatively probe the sulfation degree. All samples revealed the presence of a broad band ranging from 3000 to 3500 cm^{-1}, which can be ascribed to the OH and NH stretching region. The

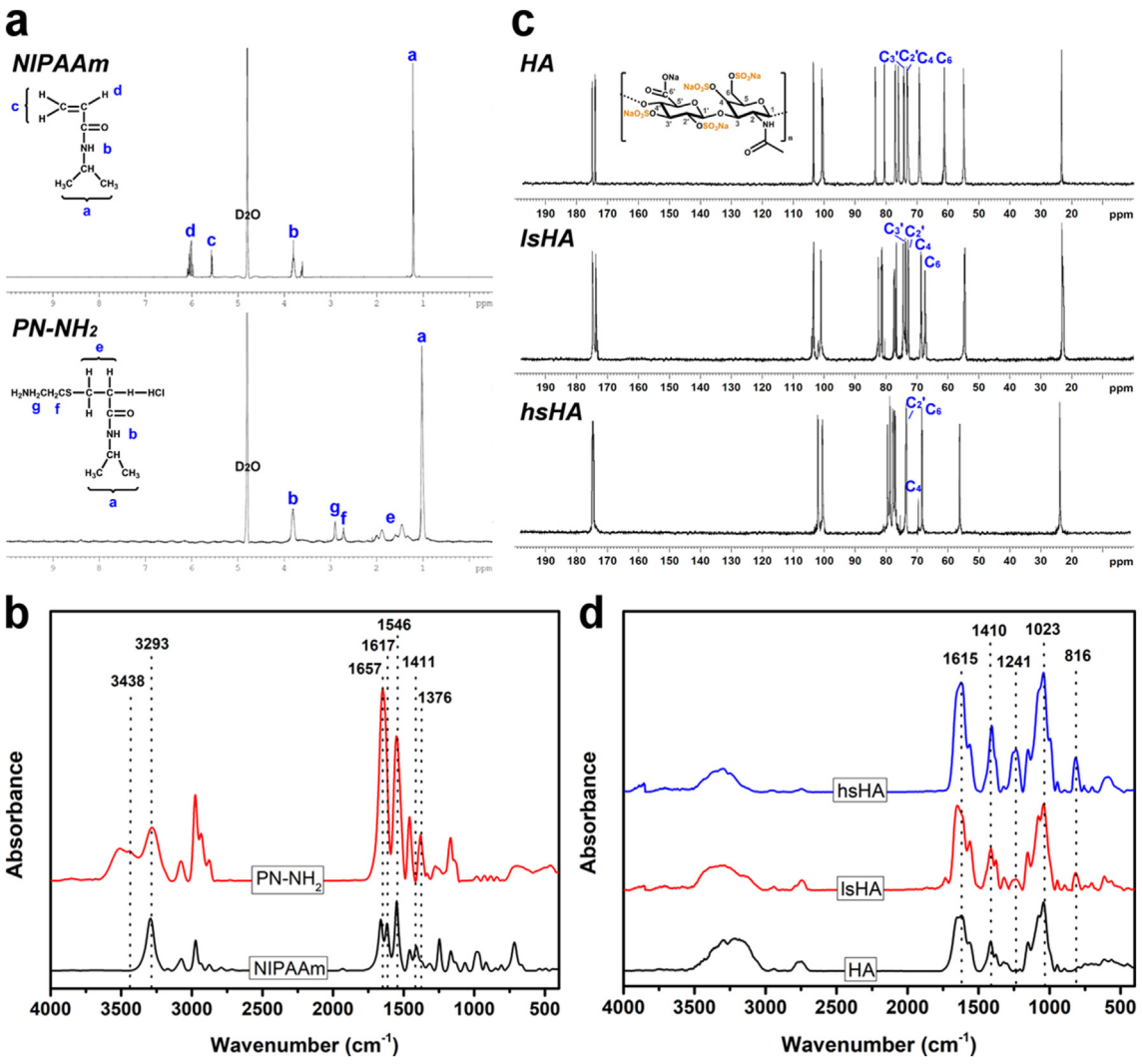

Fig. 1. Material characterizations. ^{1}H NMR (a), ^{13}C NMR (c), and FITR (b, d) spectra of the test samples including PN-NH_2, HA, lsHA, hsHA. Inclusion of NIPAAm aimed for comparison.

peak at 1615 cm^{-1} correspond to amide carbonyl while the peak at 1410 cm^{-1} is possibly due to the stretching of COO– from acid group of HA. The characteristic band at 1023 cm^{-1} can be probably attributed to the stretching mode of C-OH [49,50]. The occurrence of sulfated peaks at 1241 and 816 cm^{-1}, which are ascribed to the stretching of S═O and OSO_3^- groups, respectively, confirming the successful sulfation of the HA. It is worth noting that the relative intensity of these characteristic absorption peaks for sulfated groups increases with increasing the sulfation degree (i.e., greater intensity in hsHA specimen).

Energy dispersive spectroscopy (EDS) measurement was carried out to support the formation of the amine terminated thermo-responsive polymer and sulfated HA (Fig. S2a). The presence of nitrogen element in the EDS spectrum of the PN-NH_2 sample further confirmed the attachment of amine groups to the PN chain. There was no sulfur element in the spectrum of the HA, while obvious characteristic peaks could be found in the sulfated HA specimens. These sulfur signals and oxygen signal were more intense (compared to C signal in each spectrum) in the hsHA as compared to those of lsHA, signifying a greater sulfation degree of the hsHA (i.e., more SO_3 attached to the HA in hsHA sample). Noting that the occurrence of sulfur and chloride signals also indicates the attachment of the chain-transfer agent (containing amine group) to the PN. Moreover, zeta potential measurement was performed to probe the evolution of charge characteristics for the prepared PN-NH_2 and sulfated HA materials (Fig. S2b). The change in surface charge (from -0.8 ± 1.5 mV to 11.5 ± 2.3 mV) as the amine group introduced to the end of PN backbone additionally suggested the proper preparation of the PN-NH_2 material [51,52]. On the other hand, the negative charge nature of the HA (-28.3 ± 1.4 mV) was further enhanced with increasing the sulfation degree, possibly due to the addition of negatively charged sulfated groups [53,54]. Moreover, elemental analyzer was employed to confirm element contents and sulfation degrees in the HA and sulfated HA (Table S1). As anticipated, the degrees of sulfation in hsHA (3.2 ± 0.2 sulfate groups per disaccharide unit) are higher than those (1.3 ± 0.4 sulfate groups per disaccharide unit) in lsHA. In addition, the Mws of PN-NH_2, lsHA, and hsHA were respectively determined to be 7.8, 358, and 802 kDa; the graft yields for the copolymers were 69% (HAPN), 74% (lsHAPN), and 71% (hsHAPN). Fig. 2a shows FTIR spectra of the therapeutic thermogels after grafting sHA with PN-NH_2 via EDC/NHS coupling chemistry. Both samples reveal similar characteristic peaks as compared to their individual components (Fig. 1b and d). The formation of amide linkages can be verified by the shift of a carboxyl peak of the sHA from 1615 cm^{-1} to 1654 cm^{-1} [37]. As compared to lsHA/hsHA, the characteristic peak for OSO_3^- groups in lsHAPN/hsHAPN at 816 cm^{-1} exhibited no obvious changes, implying the grafting PN-NH_2 to sHA samples had negligible impact on the sulfation degree. To assess the possibility of the copolymers in response to temperature change, time-course UV spectroscopy was employed. Fig. 2b shows the sol-gel transition kinetics of PN-NH_2 and its combinations with HA and sHA

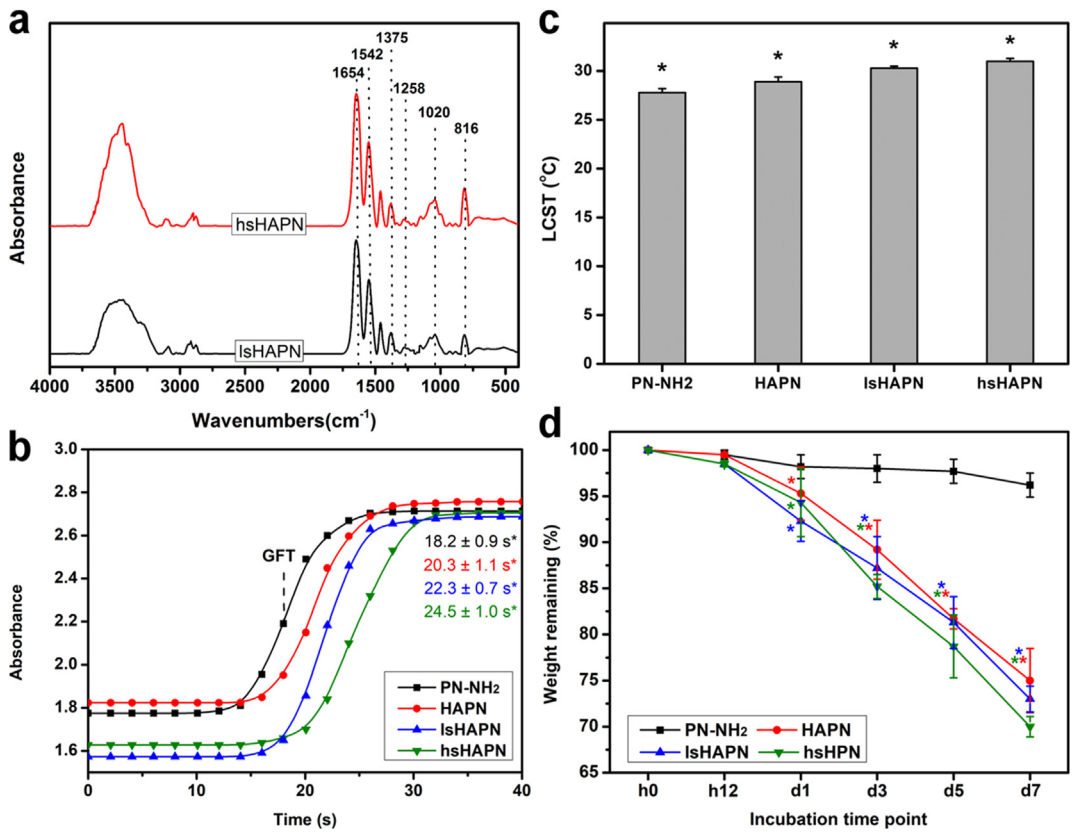

Fig. 2. Structure and property characterizations. FTIR spectra (a), gel formation time (b), LCST (c), and degradation (d) of the polymeric therapeutics. In parts (b) and (c): values are mean ± SD ($n = 5$); *$P < 0.05$ vs all groups. In part (d): The dry polymeric samples were immersed in an ATS containing 100 U/mL of hyaluronidase at 32 °C; an asterisk indicates statistically significant differences (*$P < 0.05$; $n = 5$) for the mean value of weight remaining compared to the value at previous time point.

containing different sulfation degrees (namely, HAPN, lsHAPN, and hsHAPN). The gel formation time (GFT), defined as the time at which the half absorbance of each curve, for the PN-NH_2 was 18.2 ± 0.9 s. The GFT for HAPN, lsHAPN, and hsHAPN was 20.3 ± 1.1 s, 22.3 ± 0.7 s, and 24.5 ± 1.0 s, respectively. These results imply that the copolymers with higher sulfation degrees exhibit gel formation at slower rates. The LCST of the PN-NH_2, HAPN, lsHAPN, and hsHAPN correspondingly were 27.8 ± 0.4 °C, 28.9 ± 0.5 °C, 30.3 ± 0.2 °C, and 31.0 ± 0.3 °C (Fig. 2c). This trend of increasing LCST can be ascribed to the water wettability of HA and sHA, with which the copolymers containing higher sulfation degrees possess stronger hydrophilicity and thereby greater LCST. To support these LCST data, the phase transition in response to a mimicked temperature of the ocular surface was demonstrated (Fig. S3), confirming the thermo-responsive transformation of the HAPN, lsHAPN, and hsHAPN copolymer solutions to gels. In a striking contrast, the HA polymer solution alone could not transform into gel at the ocular surface temperature (i.e., 32 °C) due to the lack of PN-NH_2 component. Furthermore, rheological properties of the copolymers were probed to confirm their sol-gel transitions (Fig. S4). For all copolymers, no viscoelastic behavior was found at the temperature below 29 °C, as verified by low moduli G' and G" (less than 1 Pa). A sharp transition can be observed in all viscoelastic shear moduli curves at transition temperatures of ~29.2 °C (HAPN), ~30.5 °C (lsHAPN), and ~31.5 °C (hsHAPN), which are consistent with the LCST values. The temperature ranges for the copolymer solutions completely transformed into gels were ~1.2 °C (HAPN), ~1.8 °C (lsHAPN), and ~2.0 °C (hsHAPN), supporting the key role of sulfate groups in regulating gelation formation (i.e., higher sulfation degrees lead to longer sol-gel transition time). Above the transition temperatures, the moduli of copolymer samples reached plateau regions (2–3 orders of magnitude increase in moduli) and revealed typical gel characteristics [55].

Considering that biodegradation is a critical factor for determining the long lasting performance of the copolymers, their biodegradability was examined (Fig. 2d). The results indicated that the weight of PN-NH_2 was slightly decreased and maintained more than 96% over a follow-up period of 7 days. In contrast, the copolymers exhibited a relatively steady weight reduction, and those with lower sulfation degrees retained greater weight percentages (~75% for the HAPN, ~73% for lsHAPN, and ~70% for hsHAPN). Such degradation can be attributed to the hydrophilicity of HA/sHA, which facilitates water diffusion and thereby smoothen the access of HA-degrading enzyme into the copolymer matrix (as compared to the PN-NH_2 matrix). Previous reports showed that the degrees of sulfation play an important role in regulating the enzymatic degradation rates of HA and HA/collagen composite hydrogels at 37 °C [56,57]. The influence of sulfate groups in the enzymatic degradation of the copolymers at 32 °C was not obvious in our study. Such a discrepancy can be attributed to the difference in structural configurations of diverse composite hydrogels. In the earlier studies, the collagen fibrils were embedded in the sHA, consequently contributing to the enzymatic resistance of sHA at negligible levels (i.e., the sulfation-mediated resistance was dominant). In this work, on the other hand, the grafting PN-NH2 segments could serve as brush barriers in limiting the invasion of hyaluronidase molecules onto the sHA/HA backbone chains at comparable extents (i.e., the PN-NH2 shield-mediated resistance was governed).

Prior to the therapeutic evaluation for the treatment of DED, ocular biocompatibility of the copolymers and their components were investigated in vitro. Fig. 3a shows phase contrast images of SIRC cells incubated with different copolymers and their individual components (test groups); SIRC cultures treated with no material served as the Ctrl group. The SIRC cells revealed healthy and characteristic morphology in all test groups, except those in the NIPAAm group. To further support these

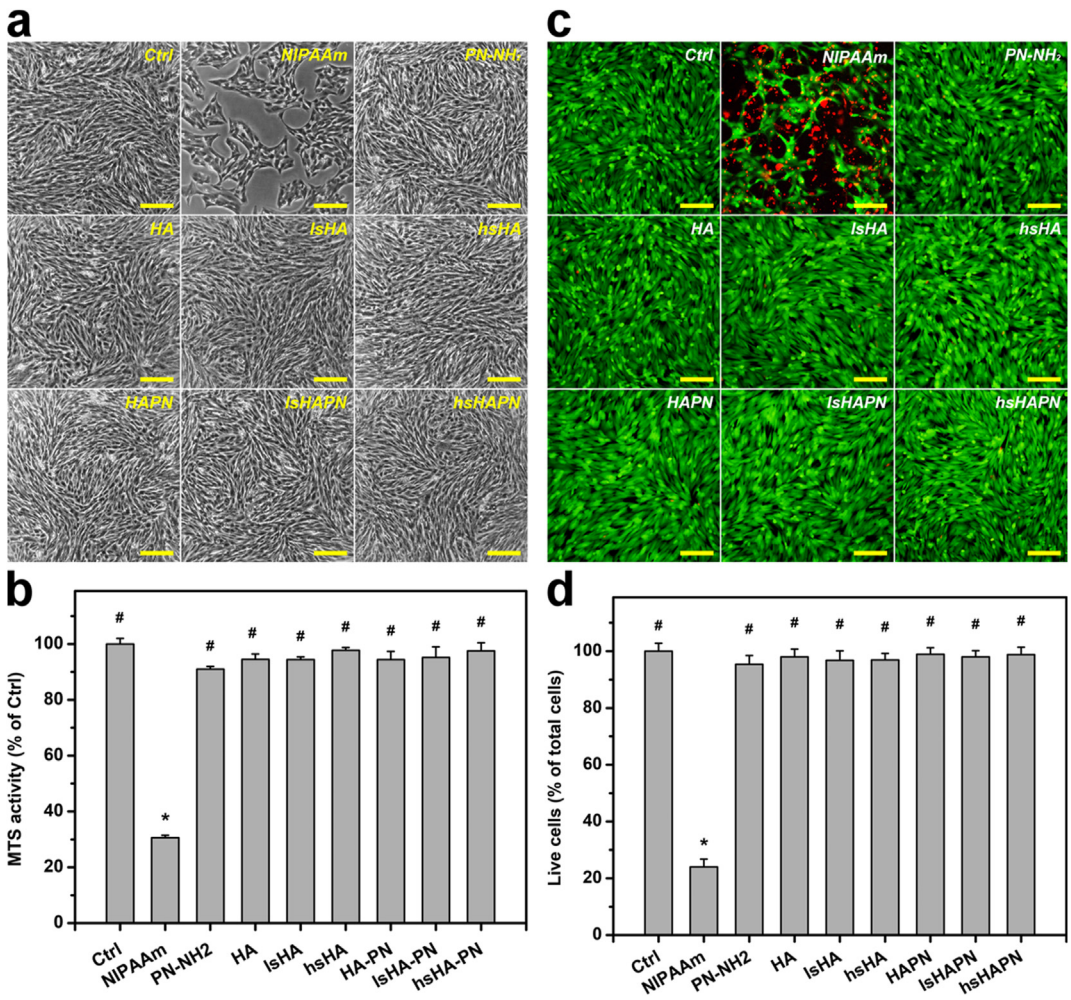

Fig. 3. In vitro biocompatibility studies. Phase contrast images (a), MTS activity (b), Live/dead staining images (c), and live cell quantification (d) of the polymeric therapeutics. In all experiments, 150 μL of the culture medium containing test mono/polymers (10% w/v) was added to the inner chamber in each SIRC cell culture well at 37 °C for 2 days. Scale bars: 100 μm. In parts (b) and (d): values are mean ± SD ($n = 6$). $^{*}P < 0.05$ vs Ctrl, PN-NH_2, HA, lsHA, hsHA, HAPN, lsHAPN, and hsHAPN groups; $^{\#}P < 0.05$ vs NIPAAm group.

morphological observation, the SIRC cell growth was assessed via a mitochondrial dehydrogenase (MTS) assay (Fig. 3b). After exposure to the test materials for 2 days, the metabolic activities for the Ctrl, NIPAAm, PN-NH_2, HA, lsHA, hsHA, HAPN, lsHAPN, and hsHAPN were 100 ± 1.9%, 30.6 ± 0.9%, 90.9 ± 0.9%, 94.4 ± 1.8%, 94.3 ± 0.9%, 97.7 ± 1.0%, 94.3 ± 2.9%, 95.1 ± 3.8%, and 97.5 ± 2.9%, respectively.

The irregular morphology and low MTS activities of SIRC cells in the NIPAAm group can be ascribed to the intrinsic cytotoxicity of the NIPAAm monomers [58]. However, the PN-NH_2 exhibited good biocompatibility, and this property was unchanged in the copolymers containing HA/sHA. Previous studies have demonstrated that the polymer forms of NIPAAm could facilitate the formation of confluent cells with healthy morphology [59]. Moreover, HA and sHA have been reported to possess excellent biocompatible and cytoprotective effects [60,61]. Accordingly, the good biocompatibility of the combined forms of HA or sHA with PN-NH_2 is perceptibly reasonable. Fig. 3c shows representative images of SIRC cells labeled with live/dead stain, where live and dead cells are perceived as green and red fluorescence, respectively. The prevalence of green signals in all cell culture groups (except NIPAAm group) infer that the test materials were harmless to the SIRC cells. These fluorescence observation was additionally reinforced by the quantitative results (Fig. 3d), confirming the non-cytotoxic nature of the developed copolymers.

Considering that inflammation is the major underlying cause of DED, it is necessary to evaluate whether the developed thermogels can attenuate elevated expression of inflammatory molecules such as IL-6, MCP-1, and TNF-α. As seen in Fig. 4a, b, and c, there were similar trends in expression of IL-6, MCP-1, and TNF-α in the inflamed SIRC cells treated with different copolymers. Healthy cells incubated with no material served as negative control (NC) group, while those induced with IL-1β worked as positive control (PC) group. High concentrations of inflammatory molecules observed in the PC group, as compared to those in NC group, indicated the effective induction of inflammation by IL-1β. As the sulfation degree was increased in the copolymers, all levels of inflammatory molecules were reduced, implying the important role of the sulfate groups in suppressing the inflammation.

The slight decrease in levels of inflammatory molecules in HAPN group can be ascribed to the HA, which has been reported to be capable of downregulating inflammatory cytokine production as well as alleviating inflammation *in vivo* [62,63]. These anti-inflammatory activities were remarkably boosted by introduction of sulfate groups, possibly due to their capability of inhibiting selectin and thereby blocking leukocyte infiltration [64]. It is worth noting that selectins can bind to sulfated sugar chains of their natural ligands such as sulfatide, a sulfated glycolipid [31,32,65]. Therefore, the inhibitory effect of the sHAPN thermogels on selectin binding was investigated in vitro by comparing their

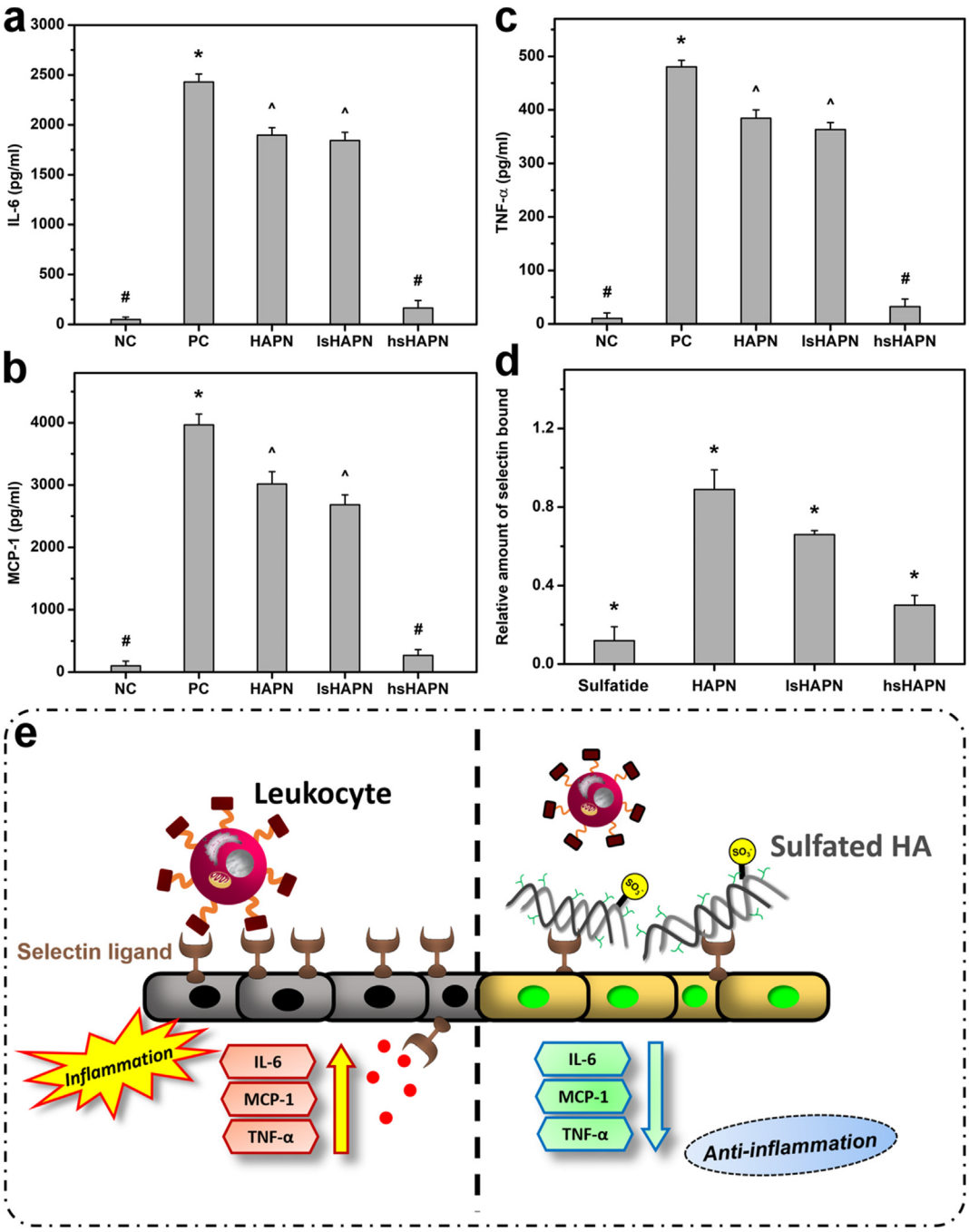

Fig. 4. Anti-inflammatory activity studies. Levels of IL-6 (a), MCP-1 (b), TNF-α (c), and relative amount of bound lectin (d). In parts (a), (b), and (c): values are mean ± SD ($n = 6$). *$P < 0.05$ vs all groups; $^{\#}P < 0.05$ vs PC, HAPN, and lsHAPN groups; $\hat{P} < 0.05$ vs NC, PC, and hsHAPN groups. In part (d): values are mean ± SD ($n = 6$). *$P < 0.05$ vs all groups; relative amount of selectin bound was quantified with a microplate reader at 490 nm with a reference correction at 630 nm. Schematic illustration (e) for the anti-inflammation mechanism of the polymeric therapeutics via selectin inhibition.

inhibition performance to sulfatide (Fig. 4d). The high amount of bound selectin in the HAPN group when comparing to the sulfatide groups signifies that the selectin was likely not blocked by the HAPN copolymer. In contrast, the selectin inhibition was increased with the addition of sulfated groups, and the higher sulfation degree in the copolymers resulted in greater inhibitory effects on selectin binding. Interestingly, the hsHAPN exhibited capability of blocking selectin as the same level as that of sulfatide, implying its potent therapeutic properties for suppressing the inflammation. Based on these in vitro results and the earlier mentioned information, a schematic illustration was proposed to elucidate a possible mechanism for the inhibition of selectin-mediated leukocyte recruitment into ocular surface and thereby the suppression of the ocular inflammation (Fig. 4e). Specifically, sulfated groups of the sHA can effectively bind to selectin ligands on the corneal epithelium, consequently preventing leukocyte infiltration and attenuating the ocular inflammation (e.g., lowering elevated levels of IL-6, MCP-1, and TNF-α inflammatory molecules).

To evaluate the therapeutic performance of the l/hsHAPN thermogels *in vivo*, an experimental model of DED induced by high-dosage topical administration of benzalkonium chloride to rabbit eyes was employed [39]. All of the rabbits afflicted with DED revealed clear signs of the ocular surface disease, including redness, tear secretion deficiency, and

inflammation. Clinically, common methods for diagnosis of DED basically rely on the observation of ocular surface abnormalities via fluorescein and rose bengal staining as well as measurement of tear secretion by Schirmer test [66,67]. Generally, the ocular surface is considered abnormal with fluorescence vital staining and rose Bengal staining scores $\geq$3, while tear secretion is deficient with wetted length $\leq$5 mm by Schirmer test without anesthesia [67]. Fig. 5a shows time course of corneal fluorescein stain images of the healthy (Pre group), as-induced DED (DED group), artificial tear solution (ATS)-treated DED (Ctrl group) and copolymer-treated DED (HAPN, lsHAPN, and hsHAPN groups) rabbit eyes for a follow-up period of 7 days. It is clearly seen that there is almost no fluorescein stain absorbed on the healthy eye, suggesting the defect-free ocular surface in the Pre group. On the other hand, the as-induced DED eyes revealed a positive fluorescein pattern which fully enveloped the corneal region, signifying the manifestation of defects in the corneal epithelium. Single topical administration of ATS on the DED eyes had no impact on alleviating the disease progression, as implied by the prevalent increase of the green fluorescence signals (Ctrl group, 12 h to 7 d post-instillation). The fluorescein patterns in the diseased eyes treated with the thermogels (single dose) showed different appearances with respect to the sulfation degrees. As compared to the Ctrl group, there was a slight reduction of green fluorescence signals in the HAPN group, suggesting a slight therapeutic effect generated by the non-sulfated thermogel. This minimal therapeutic efficacy can be attributed to the HA molecules from degraded HAPN, which trigger their intrinsic anti-inflammatory activity and thereby suppress the ocular inflammation [68]. As anticipated, adding a sufficient amount of sulfate groups to the HAPN could lead to the significant improvement in treatment efficacy. In particular, the hsHAPN could gradually reduce the prevalence of the green fluorescence signals close to the level of healthy eyes after 7 days. This lifelong and high treatment efficacy of the hsHAPN can be ascribed to the synergistic combination between the slow degradation of the copolymer via the temperature-induced gelation and the adequate quantity of sulfate groups. This could lead to a strong interaction with selectins and to the hindrance of selectin from binding to leukocytes for a prolonged time as suggest by the in vitro results, consequently preventing leukocyte infiltration and alleviating the inflamed ocular surface.

In addition, quantitative results of the corneal fluorescein staining were also analyzed (Fig. 5b). No obvious changes in the scores of the HAPN and lsHAPN groups were recorded during the follow-up, suggesting these two copolymers could only prevent the DED progression at minimal-to-moderate therapeutic efficacy. In a striking contrast, the time-course score of the hsHAPN group showed a gradual decrease and reduced to below the DED threshold score at day 7 post-instillation (~4-fold decrease, as compared to the Ctrl group). Rose bengal staining was also examined on the animal eyes for diagnosing the damage and recovery of the ocular surfaces [69]. As shown in Fig. 5c, rose bengal stain could not be detected in the healthy ocular surface since the eyes at preoperation (Pre group) had no epithelial defects that could trap the

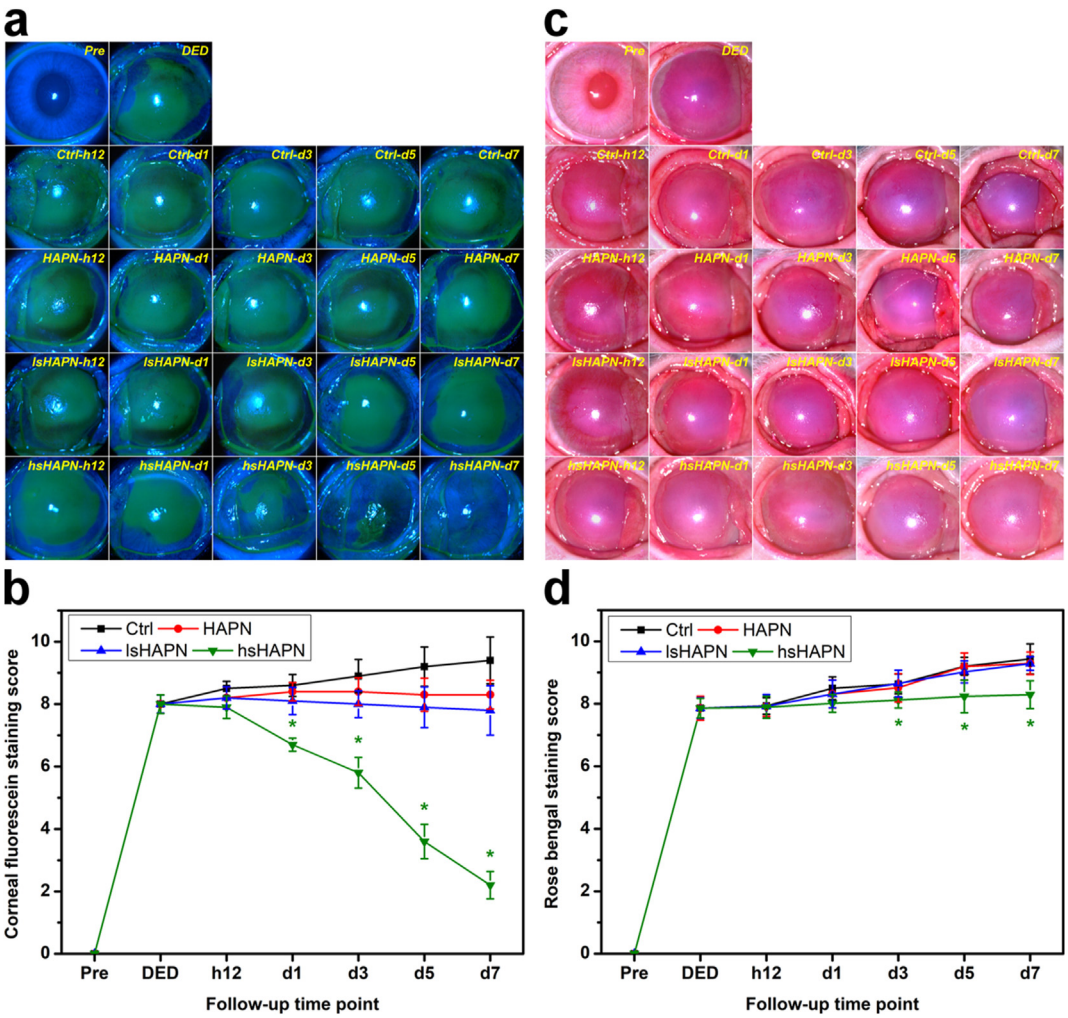

Fig. 5. Clinical observations. Corneal fluorescein staining images and scores (a–b) and rose bengal staining images and scores (c–d) of healthy (Pre), as-induced (DED), and DED rabbit eyes treated with polymeric therapeutics (HAPN, lsHAPN, hsHAPN). DED animals receiving ATS only served as a control group (Ctrl). Asterisks indicate statistically significant differences (*$P < 0.05$; $n = 6$) as compared with the Ctrl groups. Follow-up time point: hour (h); day (d).

stain. In the DED group, positive rose bengal stain signals were prominently visualized, implying the occurrence of abnormalities in the preocular tear film. After single-dose instillation, the rose bengal stain coverage slightly increased in all groups, except the hsHAPN. Quantitative results on the rose bengal stains were shown in Fig. 5d, revealing a good agreement with the qualitative observation. Although hsHAPN copolymer could alleviate the inflamed ocular surface, it revealed negligible role in promoting the corneal goblet cells to secrete mucus for generation of a protective mucus layer, as signified by the relative high scores (above 3). Therefore, for a complete alleviation of ocular surface inflammation and its complication such as the mucin-deficiency, future studies on the incorporation of hsHAPN with an additional agent that can promote the mucin secretion of goblet cells is necessary. Therapeutic effects of the copolymers on the treatment of tear deficiency in the diseased eyes were further assessed by Schirmer test, a quantitative measurement of tear secreted by the lacrimal gland [70]. Based on this diagnosis, the wetted lengths from the paper strips positioned in the cul-de-sac for 3 min in the test rabbit eyes were quantified (Fig. S5). The wetted length of 12.0 ± 0.21 mm in the Pre group implies the normal tear secretion in healthy eyes [67], while reduced wetted length of 5.0 ± 0.22 mm in the DED group indicates tear deficiency of the diseased eyes. Further decrease in wetted lengths was found in Ctrl, HAPN, and lsHAPN groups at 7 days post-instillation, inferring the negligible or insufficient efficacies. In contrast, the wetted length of 5.3 ± 0.26 mm in the hsHAPN group further support the highest treatment efficacy could be obtained by the hsHAPN therapeutic copolymer. Collectively, the staining and tear examinations demonstrate that the hsHAPN, owing to its highest selectin-inhibitory effect, can provide an efficient prevention of leukocyte infiltration as implied by the in vitro studies, consequently impeding the progression of corneal damage and tear secretion deficiency in the DED eyes.

It is known that inflammation is a major contributor to the reduction of corneal thickness and disruption of epithelium and stroma, leading to the damage of the cornea in the DED eyes [71]. In this regard, hematoxylin and eosin (H&E) staining was employed to examine histological changes of the cornea in response to the topically applied thermogels. The epithelium layer (E) and the stroma (S) in the cornea of healthy eyes were well organized and firmly attached together, and the corneal surface was smooth (Fig. 6a). Abnormalities such as disrupted epithelium and stroma could be found in the cornea of as-induced DED eyes. At 7 days post-instillation of ATS, the corneal epithelium layers in the DED eyes revealed thinner and more disordered structures, signifying the ineffective therapeutic performance of the formulation. Single-dose administration of the copolymer formulations showed a strong correlation between the sulfate amount and treatment efficacy. Notably, the hsHAPN formulation could recover the defective corneal epithelium and stroma layers close to their normal states. The corneal epithelium thickness was also quantified (Fig. 6b) based on the H&E staining images. Specifically, the thickness of corneal epithelium in the healthy eyes (Pre group) was estimated to be 48.0 ± 4.6 μm, which is consistent with previously reported data [72]. The thickness was significantly reduced in DED eyes (24.5 ± 5.0 μm) and deeply decreased in the ATS-treated DED eyes (10.0 ± 3.1 μm). The slight decrease of the epithelium thickness in the HAPN and lsHAPN groups as compared to that in the DED group suggests the treatment using the copolymers with zero and low sulfation degree could provide a certain therapeutic activity to prevent the DED progression.

There is no obvious difference in the epithelium thicknesses between the hsHAPN (47.1 ± 7.2 μm) and Pre groups, validating the tissue impairment was suppressed and the cornea structure was repaired (accounting for ~99% thickness recovery) by the copolymer containing sufficient amount of sulfate groups.

Ocular surface inflammation has been reported as a cause of corneal cell apoptosis in several DED models [73,74]. Accordingly, therapeutic effects of the thermogels on cellular apoptosis in the diseased rabbit eyes were further investigated. To this end, corneal tissue sections from the test animals were inspected using terminal deoxynucleotidyl transferase (TdT)-mediated dUTP nick end labeling (TUNEL) and 4′,6-diamidino-2-phenylindole (DAPI) assays. Fig. 6c shows fluorescence microscopic images of different corneal tissue sections co-stained with

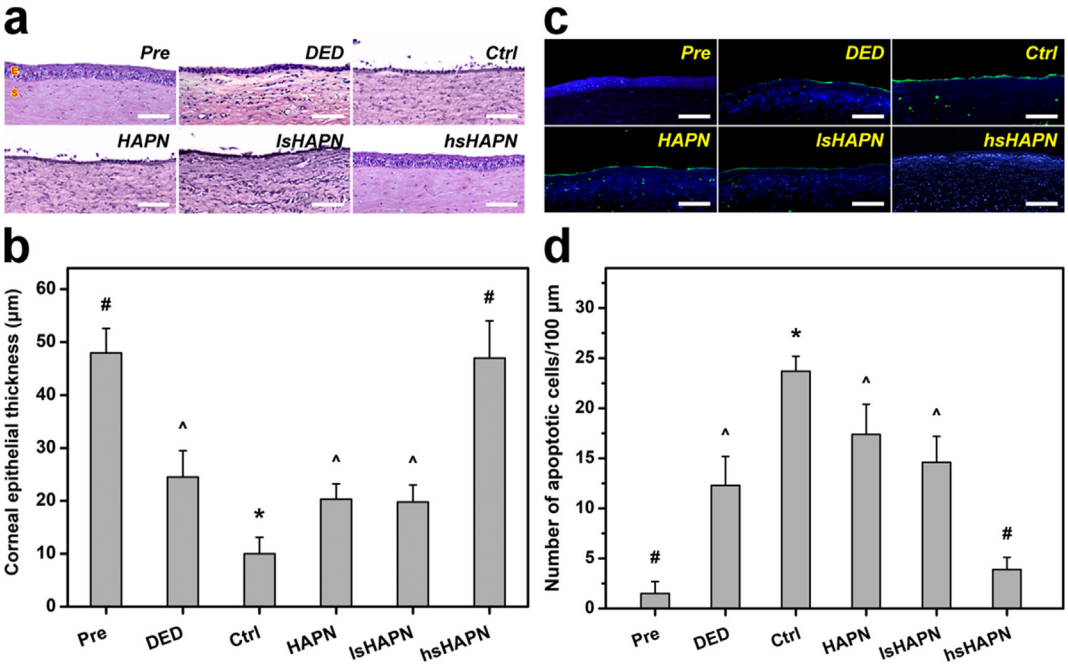

Fig. 6. Histological studies. Histological images (a), thickness values (b), fluorescence images (c), and apoptotic cell numbers (d) of corneal epithelium in healthy (Pre), as-induced (DED), and DED rabbit eyes treated with polymeric therapeutics (HAPN, lsHAPN, hsHAPN). DED animals receiving ATS only served as the control group (Ctrl). Sections are stained with H&E (a) and TUNEL and DAPI (c). Scale bars: 100 μm. (a) E: epithelium; S: stroma. (c) Blue fluorescence is DAPI nuclei staining. Green fluorescence is TUNEL-positive nuclei staining. In parts (b) and (d): values are mean ± SD ($n = 6$). $^{*}P < 0.05$ vs all groups; $^{\#}P < 0.05$ vs DED, Ctrl, HAPN, and lsHAPN groups; $^{\wedge}P < 0.05$ vs Pre, Ctrl, and hsHAPN groups.

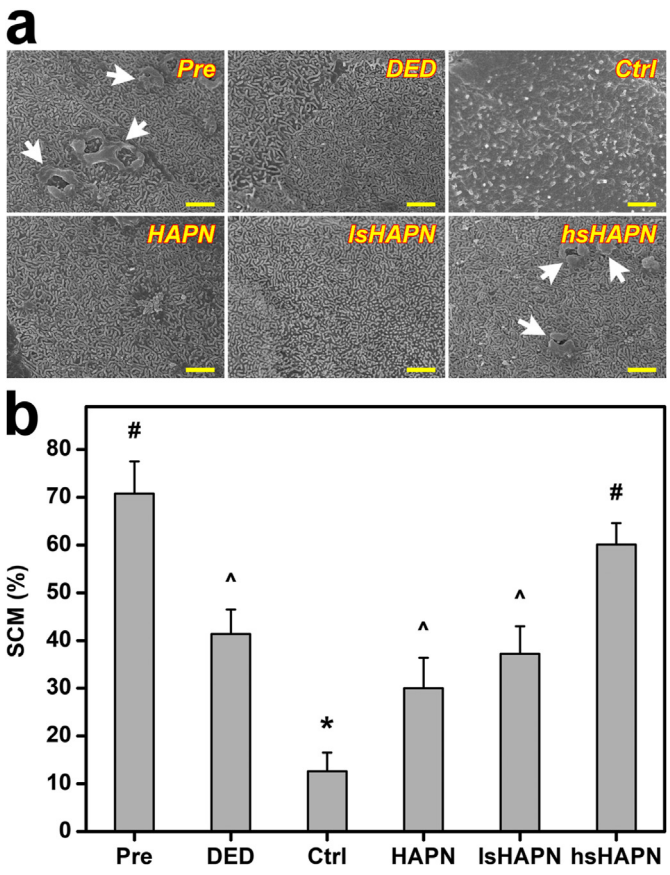

Fig. 7. Morphological studies. (a) Representative SEM images of microvilli on corneal epithelial cell surfaces and (b) corneal epithelial cell surface covered by microvilli (SCM) values in different groups. Scale bars: 1 μm. White arrows in part (a) indicate the micro-structural folds. Values are mean ± SD ($n = 6$). $^{*}P <$ 0.05 vs all groups; $^{\#}P < 0.05$ vs DED, Ctrl, HAPN, and lsHAPN groups; $\hat{P} < 0.05$ vs Pre, Ctrl, and hsHAPN groups.

TUNEL (green) and DAPI (blue). The comparable expression of green fluorescence signals, which characterized TUNEL-labeled apoptotic cells, in the DED, HAPN, and lsHAPN groups indicates the poor therapeutic efficacy of the copolymers with non/insufficient sulfate groups. The fluorescence expression even became more prevalent in the Ctrl group, signifying the ATS formulation could not preclude the DED development. In a striking contrast, the negligible green fluorescence displayed in the hsHAPN groups demonstrates the effective attenuation of apoptotic cells from the copolymer with high sulfation degree via initiating their potent anti-inflammatory activity in the test corneas. In addition, the results on apoptotic corneal epithelial cells were also quantified (Fig. 6d), exhibiting a similar trend in expression of cellular apoptosis in response to treatment efficacy of different formulations. The number of apoptotic cells per 100 μm length of the corneal epithelial layer in the healthy rabbits was estimated to be as low as 1.5 ± 1.2 (cells/100 μm). In the corneas of DED eyes, this number was increased to 12.3 ± 2.9 (cells/100 μm), which is well agreed with the results from other experimental models [75,76]. The number of apoptotic cells was considerably higher (23.7 ± 1.5 cells/100 μm) in the Ctrl group, confirming the single-dose ATS formulation had no therapeutic impact during the follow-up period. The sulfation-dependent treatment efficacy was apparently recognized by the decrease in apoptotic cells with the increasing of the sulfation degree in the copolymers. Noting that the apoptotic cells (3.9 ± 1.1 cells/100 μm) in the hsHAPN group was closely comparable to that in the Pre group, signifying the highest treatment efficacy (corresponding to ~68.3% cells recovered) of the copolymer containing sufficiently high sulfate amount.

On the corneal surface, microvilli are an important structural component that maintains the adhesion between tear film and epithelial cells, and any damage to the microvilli (thus, microvilli density reduction) can cause the dehydration in the eye [77,78]. Because of the sensitive response of microvilli to the external stimuli, changes in microvilli can be utilized as a marker for evaluation of ocular surface health [79]. In this regard, the morphological and structural changes of the microvilli of the DED eyes with respect to the treatment using the different copolymer formulations were investigated. Fig. 7a indicates SEM images of the corneal epithelial surface of different test rabbit eyes.

In the Pre group, the microvilli possessed healthy morphology and structure, as indicated by their normal length and regular organization as well as the presence of micro-structural folds on the corneal surface. The microvilli became shorter and disordered, and the micro-structural folds disappeared in the eyes induced with DED. These irregular characteristics were more identifiable in the ATS-treated DED eyes with a distinct reduction of microvilli coverage (Ctrl group). Interestingly, the microvilli characteristics and micro-structural folds were restored in the diseased eyes treated with the copolymers. The highest recovery effect offered by the hsHAPN can be ascribed to its capability of providing the therapeutic sHA molecules with strongest anti-inflammatory activity during the follow-up period. The microvilli coverage on corneal epithelial surface in the test animals was further quantitatively analyzed (Fig. 7b) as a general assessment of the microvilli length and density. The surface coverage percentage for the Pre group was as high as 70.8 ± 6.7%, and this value was gradually decreased to 41.4 ± 5.1% (DED group) and 12.6 ± 3.9% (Ctrl group). Treatments with the therapeutic agents could help to prevent the progressive loss of the microvilli (30.0 ± 6.4% and 37.2 ± 7.8% for the HAPN and lsHAPN groups, respectively) and eventually restore the microvilli coverage of the corneal epithelial surface up to ~85% (60.1 ± 4.5% for the hsHAPN group). These results reflect the key role of sulfation degree of the therapeutic copolymers in repairing the microvilli and micro-structural folds, consequently achieving the healthy structure of the corneal epithelial cell surface and mitigating the DED eyes.

4. Conclusions

In summary, we have developed an efficient therapeutic thermogel for the treatment of corneal inflammation via a rational exploitation of HAPN copolymers containing different sulfate amounts. The therapeutic agent is thermo-responsive to the ocular surface and high biocompatible to corneal cells and is capable of delivering sHA at least for 7 days, consequently exerting potent anti-inflammatory and prolonged therapeutic activities on the corneal region. *In vivo* studies suggest that single-dose topical instillation of the hsHAPN formulation could repair corneal epithelial defects, prevent cell apoptosis, and suppress ocular surface inflammation for a follow-up period of 7 days. This high treatment efficacy can be ascribed to the inhibitory effects of the hsHAPN copolymer on selectin-mediated leukocyte infiltration as well as corneal-protective properties of sHA molecules. Overall, this study may provide a promising future use of sHAPN as an exciting thermo-responsive carrier for improving ocular bioavailability of various ophthalmic drugs while offering imperative therapeutic benefits such as anti-inflammation and corneal protection.

Credit author statement

Duc Dung Nguyen: Data Curation, Formal analysis, Writing - Original Draft, Writing - Review & Editing, Li-Jyuan Luo: Conceptualization, Investigation, Writing - Original Draft, Jui-Yang Lai: Conceptualization, Methodology, Visualization, Validation, Writing - Review & Editing, Supervision, Project administration, Funding acquisition.

Data availability statement

The raw/processed data required to reproduce these findings cannot be shared at this time as the data also forms part of an ongoing study.

Declaration of competing interest

The authors declare that they have no known competing financial interests or personal relationships that could have appeared to influence the work reported in this paper.

Acknowledgements

The research was financially supported by grants MOST110-2221-E-182-023-MY3 and MOST110-2811-E-182-505 from the Ministry of Science and Technology of Republic of China; grants CMRPD2L0021 and CMRPD2L0161 from Chang Gung Memorial Hospital, Linkou; and grant NHRI-EX110-10826EI from the National Health Research Institutes of Taiwan.

Appendix A. Supplementary data

Supplementary data to this article can be found online at https://doi.org/10.1016/j.mtbio.2021.100183.

References

[1] J.K. Portello, M. Rosenfield, C.A. Chu, Blink rate, incomplete blinks and computer vision syndrome, Optom. Vis. Sci. 90 (2013) 482–487.
[2] J. Ding, D.A. Sullivan, Aging and dry eye disease, Exp. Gerontol. 47 (2012) 483–490.
[3] D.D. Nguyen, J.Y. Lai, Advancing the stimuli response of polymer-based drug delivery systems for ocular disease treatment, Polym. Chem. 11 (2020) 6988–7008.
[4] M.T.M. Wang, A. Muntz, J. Lim, J.S. Kim, L. Lacerda, A. Arora, J.P. Craig, Ageing and the natural history of dry eye disease: a prospective registry-based cross-sectional study, Ocul. Surf. 18 (2020) 736–741.
[5] J. Yu, C.V. Asche, C.J. Fairchild, The economic burden of dry eye disease in the United States: a decision tree analysis, Cornea 30 (2011) 379–387.
[6] J.A. Clayton, Dry eye, N, Engl. J. Med. 378 (2018) 2212–2223.
[7] B. Pouyeh, E. Viteri, W. Feuer, D.J. Lee, H. Florez, J.A. Fabian, V.L. Perez, A. Galor, Impact of ocular surface symptoms on quality of life in a United States veterans affairs population, Am. J. Ophthalmol. 153 (2012) 1061–1066.
[8] M.L. Massingale, X. Li, M. Vallabhajosyula, D. Chen, Y. Wei, P.A. Asbell, Analysis of inflammatory cytokines in the tears of dry eye patients, Cornea 28 (2009) 1023–1027.
[9] D. Acar, I.T. Molina-Martínez, M. Gómez-Ballesteros, M. Guzmán-Navarro, J.M. Benítez-Del-Castillo, R. Herrero-Vanrell, Novel liposome-based and in situ gelling artificial tear formulation for dry eye disease treatment, Contact Lens Anterior Eye 41 (2018) 93–96.
[10] C.S. de Paiva, S.C. Pflugfelder, S.M. Ng, E.K. Akpek, Topical cyclosporine A therapy for dry eye syndrome, Cochrane Database Syst. Rev. 9 (2019), CD010051.
[11] R. Gaudana, J. Jwala, S.H. Boddu, A.K. Mitra, Recent perspectives in ocular drug delivery, Pharm. Res. (N. Y.) 26 (2009) 1197–1216.
[12] L.D. Barber, S.C. Pflugfelder, J. Tauber, G.N. Foulks, Phase III safety evaluation of cyclosporine 0.1% ophthalmic emulsion administered twice daily to dry eye disease patients for up to 3 years, Ophthalmology 112 (2005) 1790–1794.
[13] K.S. Kunert, A.S. Tisdale, M.E. Stern, J.A. Smith, I.K. Gipson, Analysis of topical cyclosporine treatment of patients with dry eye syndrome: effect on conjunctival lymphocytes, Arch. Ophthalmol. 118 (2000) 1489–1496.
[14] S.K. Chauhan, R. Dana, Role of Th17 cells in the immunopathogenesis of dry eye disease, Mucosal Immunol. 2 (2009) 375–376.
[15] M.E. Stern, J. Gao, T.A. Schwalb, M. Ngo, D.D. Tieu, C.C. Chan, B.L. Reis, S.M. Whitcup, D. Thompson, J.A. Smith, Conjunctival T-cell subpopulations in Sjögren's and non-Sjögren's patients with dry eye, Invest. Ophthalmol. Vis. Sci. 43 (2002) 2609–2614.
[16] D.T. Jones, D. Monroy, Z. Ji, S.S. Atherton, S.C. Pflugfelder, Sjögren's syndrome: cytokine and Epstein-Barr viral gene expression within the conjunctival epithelium, Invest. Ophthalmol. Vis. Sci. 35 (1994) 3493–3504.
[17] S.C. Pflugfelder, D. Jones, Z. Ji, A. Afonso, D. Monroy, Altered cytokine balance in the tear fluid and conjunctiva of patients with Sjögren's syndrome keratoconjunctivitis sicca, Curr. Eye Res. 19 (1999) 201–211.
[18] M. Tishler, I. Yaron, Q. Geyer, I. Shirazi, E. Naftaliev, M. Yaron, Elevated tear interleukin-6 levels in patients with Sjögren's syndrome, Ophthalmology 105 (1998) 2327–2329.
[19] M. Rolando, S. Barabino, C. Mingari, S. Moretti, S. Giuffrida, G. Calabria, Distribution of conjunctival HLA-DR expression and the pathogenesis of damage in early dry eye, Cornea 24 (2005) 951–954.
[20] R.M. Corrales, A. Villarreal, W. Farley, M.E. Stern, D.Q. Li, S.C. Pflugfelder, Strain-related cytokine profiles on the murine ocular surface in response to desiccating stress, Cornea 26 (2007) 579–584.
[21] M. Kawashima, T. Kawakita, T. Inaba, N. Okada, M. Ito, S. Shimmura, M. Watanabe, K. Shinmura, K. Tsubota, Dietary lactoferrin alleviates age-related lacrimal gland dysfunction in mice, PLoS One 7 (2012), e33148.
[22] Y. Wei, P.A. Asbell, The core mechanism of dry eye disease is inflammation, Eye Contact Lens 40 (2014) 248–256.
[23] H.D. Perry, R. Solomon, E.D. Donnenfeld, A.R. Perry, J.R. Wittpenn, H.E. Greenman, H.E. Savage, Evaluation of topical cyclosporine for the treatment of dry eye disease, Arch. Ophthalmol. 126 (2008) 1046–1050.
[24] J.P. Kersey, D.C. Broadway, Corticosteroid-induced glaucoma: a review of the literature, Eye 20 (2006) 407–416.
[25] M.L. Ratay, S.C. Balmert, A.P. Acharya, A.C. Greene, T. Meyyappan, S.R. Little, TRI Microspheres prevent key signs of dry eye disease in a murine, inflammatory model, Sci. Rep. 7 (2017), 17527.
[26] P.J. Gillies, N.A. Richardson, J. Walshe, S.A. Stephenson, R.A. Dawson, D.G. Harkin, Demonstration of P-selectin expression and potential function in human corneal epithelial cells, Exp. Eye Res. 176 (2018) 196–206.
[27] I.C. You, Y. Li, R. Jin, M. Ahn, W. Choi, K.C. Yoon, Comparison of 0.1%, 0.18%, and 0.3% hyaluronic acid eye drops in the treatment of experimental dry eye, J. Ocul. Pharmacol. Therapeut. 34 (2018) 557–564.
[28] M.E. Johnson, P.J. Murphy, M. Boulton, Effectiveness of sodium hyaluronate eye drops in the treatment of dry eye, Graefes Arch. Clin. Exp. Ophthalmol. 244 (2006) 109–112.
[29] X. Zhang, D. Wei, Y. Xu, Q. Zhu, Hyaluronic acid in ocular drug delivery, Carbohydr. Polym. 264 (2021), 118006.
[30] W.H. Chang, P.Y. Liu, M.H. Lin, C.J. Lu, H.Y. Chou, C.Y. Nian, Y.T. Jiang, Y.H.H. Hsu, Applications of hyaluronic acid in ophthalmology and contact lenses, Molecules 26 (2021), 2485.
[31] M.S. Mulligan, R.L. Warner, J.B. Lowe, P.L. Smith, Y. Suzuki, M. Miyasaka, S. Yamaguchi, Y. Ohta, Y. Tsukada, M. Kiso, A. Hasegawa, P.A. Ward, In vitro and in vivo selectin-blocking activities of sulfated lipids and sulfated sialyl compounds, Int. Immunol. 10 (1998) 569–575.
[32] M. Matsuda, K. Shikata, F. Shimizu, Y. Suzuki, M. Miyasaka, H. Kawachi, H. Kawashima, J. Wada, H. Sugimoto, Y. Shikata, D. Ogawa, S.J. Tojo, K. Akima, H. Makino, Therapeutic effect of sulphated hyaluronic acid, a potential selectin-blocking agent, on experimental progressive mesangial proliferative glomerulonephritis, J. Pathol. 198 (2002) 407–414.
[33] D. Ogawa, K. Shikata, M. Matsuda, K. Akima, M. Iwahashi, S. Okada, Y. Tsuchiyama, Y. Shikata, J. Wada, H. Makino, Sulfated hyaluronic acid, a potential selectin inhibitor, ameliorates experimentally induced crescentic glomerulonephritis, Nephron Exp. Nephrol. 99 (2005) e26–e32.
[34] S. Al-Maawi, S. Rother, N. Halfter, K.M. Fiebig, J. Moritz, S. Moeller, M. Schnabelrauch, C.J. Kirkpatrick, R. Sader, H.P. Wiesmann, D. Scharnweber, V. Hintze, S. Ghanaati, Covalent linkage of sulfated hyaluronan to the collagen scaffold Mucograft® enhances scaffold stability and reduces proinflammatory macrophage activation in vivo, Bioact. Mater. 8 (2022) 420–434.
[35] V. Hintze, S. Moeller, M. Schnabelrauch, S. Bierbaum, M. Viola, H. Worch, D. Scharnweber, Modifications of hyaluronan influence the interaction with human bone morphogenetic protein-4 (hBMP-4), Biomacromolecules 10 (2009) 3290–3297.
[36] J.Y. Lai, A.C. Hsieh, A gelatin-g-poly(N-isopropylacrylamide) biodegradable in situ gelling delivery system for the intracameral administration of pilocarpine, Biomaterials 33 (2012) 2372–2387.
[37] D.I. Ha, S.B. Lee, M.S. Chong, Y.M. Lee, Preparation of thermo-responsive and injectable hydrogels based on hyaluronic acid and poly(N-isopropylacrylamide) and their drug release behaviors, Macromol. Res. 14 (2006) 87–93.
[38] L.A. Wells, S. Furukawa, H. Sheardown, Photoresponsive PEG-anthracene grafted hyaluronan as a controlled-delivery biomaterial, Biomacromolecules 12 (2011) 923–932.
[39] C. Xiong, D. Chen, J. Liu, B. Liu, N. Li, Y. Zhou, X. Liang, P. Ma, C. Ye, J. Ge, Z. Wang, A rabbit dry eye model induced by topical medication of a preservative benzalkonium chloride, Invest. Ophthalmol. Vis. Sci. 49 (2008) 1850–1856.
[40] K. Tsubota, H. Fujita, K. Tsuzaka, T. Takeuchi, Mikulicz's disease and Sjogren's syndrome, Invest. Ophthalmol. Vis. Sci. 41 (2000) 1666–1673.
[41] S. Burgalassi, L. Panichi, P. Chetoni, M.F. Saettone, E. Boldrini, Development of a simple dry eye model in the albino rabbit and evaluation of some tear substitutes, Ophthalmic Res. 31 (1999) 229–235.
[42] Z. Mao, L. Ma, J. Yan, M. Yan, C. Gao, J. Shen, The gene transfection efficiency of thermoresponsive N, N, N-trimethyl chitosan chloride-g-poly (N-isopropyl acrylamide) copolymer, Biomaterials 28 (2007) 4488–4500.
[43] P. Patra, A.P. Rameshbabu, D. Das, S. Dhara, A.B. Panda, P. Sagar, Stimuli-responsive, biocompatible hydrogel derived from glycogen and poly(N-isopropylacrylamide) for colon targeted delivery of ornidazole and 5-amino salicylic acid, Polym. Chem. 7 (2016) 5426–5435.
[44] C. Boyer, C. Loubat, J.J. Robin, B. Boutevin, Synthesis of functionalized amine oligomers by free-radical telomerization of methyl methacrylate with a peculiar telogen: 2-Aminoethanethiol hydrochloride, J. Polym. Sci., Polym. Chem. Ed. 42 (2004) 5146–5160.
[45] N. Milašinović, Z. Knežević-Jugović, N. Milosavljević, M. Lučić Škorić, J. Filipović, M. Kalagasidis Krušić, Stimuli-sensitive hydrogel based on N-isopropylacrylamide and itaconic acid for entrapment and controlled release of Candida rugosa lipase under mild conditions, BioMed Res. Int. 2014 (2014), 364930.
[46] B. Baghaei, S.H. Jafari, H.A. Khonakdar, U. Wagenknecht, G. Heinrich, Novel thermosensitive hydrogel composites based on poly(D,L-lactide-co-glycolide)

nanoparticles embedded in poly(N-isopropyl acrylamide) with sustained drug-release behavior, J. Appl. Polym. Sci. 131 (2014), 40625.
[47] D.K. Lim, R.G. Wylie, R. Langer, D.S. Kohane, Selective binding of C-6 OH sulfated hyaluronic acid to the angiogenic isoform of VEGF(165), Biomaterials 77 (2016) 130–138.
[48] A. Magnani, S. Lamponi, R. Rappuoli, R. Barbucci, Sulphated hyaluronic acids: a chemical and biological characterization, Polym. Int. 46 (1998) 225–240.
[49] Y. Wu, Preparation of low-molecular-weight hyaluronic acid by ozone treatment, Carbohydr. Polym. 89 (2012) 709–712.
[50] S.A. de Oliveira, B.C. da Silva, I.C. Riegel-Vidotti, A. Urbano, P.C. de Sousa Faria-Tischer, C.A. Tischer, Production and characterization of bacterial cellulose membranes with hyaluronic acid from chicken comb, Int. J. Biol. Macromol. 97 (2017) 642–653.
[51] C. Echeverría, A. Aragón-Gutiérrez, M. Fernández-García, A. Muñoz-Bonilla, D. López, Thermoresponsive poly(N-isopropylacrylamide-co-dimethylaminoethyl methacrylate) microgel aqueous dispersions with potential antimicrobial properties, Polymers 11 (2019), 606.
[52] P. Mesquida, D. Kohl, O.G. Andriotis, P.J. Thurner, M. Duer, S. Bansode, G. Schitter, Evaluation of surface charge shift of collagen fibrils exposed to glutaraldehyde, Sci. Rep. 8 (2018), 10126.
[53] P. Maudens, S. Meyer, C.A. Seemayer, O. Jordan, E. Allémann, Self-assembled thermoresponsive nanostructures of hyaluronic acid conjugates for osteoarthritis therapy, Nanoscale 10 (2018) 1845–1854.
[54] B.P. Purcell, I.L. Kim, V. Chuo, T. Guinen, S.M. Dorsey, J.A. Burdick, Incorporation of sulfated hyaluronic acid macromers into degradable hydrogel scaffolds for sustained molecule delivery, Biomater. Sci. 2 (2014) 693–702.
[55] B.L. Ekerdt, C.M. Fuentes, Y. Lei, M.M. Adil, A. Ramasubramanian, R.A. Segalman, D.V. Schaffer, Thermoreversible hyaluronic acid-PNIPAAm hydrogel systems for 3D stem cell culture, Adv. Healthc. Mater. 7 (2018), 1800225.
[56] S. Rother, V.D. Galiazzo, D. Kilian, K.M. Fiebig, J. Becher, S. Moeller, U. Hempel, M. Schnabelrauch, J. Waltenberger, D. Scharnweber, V. Hintze, Hyaluronan/collagen hydrogels with sulfated hyaluronan for improved repair of vascularized tissue tune the binding of proteins and promote endothelial cell growth, Macromol. Biosci. 17 (2017), 1700154.
[57] K. Lemmnitzer, J. Schiller, J. Becher, S. Möller, M. Schnabelrauch, Improvement of the digestibility of sulfated hyaluronans by bovine testicular hyaluronidase: a UV spectroscopic and mass spectrometric study, BioMed Res. Int. 2014 (2014), 986594.
[58] M.A. Cooperstein, H.E. Canavan, Assessment of cytotoxicity of (N-isopropyl acrylamide) and poly(N-isopropyl acrylamide)-coated surfaces, Biointerphases 8 (2013) 19.
[59] J.Y. Lai, K.H. Chen, W.M. Hsu, G.H. Hsiue, Y.H. Lee, Bioengineered human corneal endothelium for transplantation, Arch. Ophthalmol. 24 (2006) 1441–1448.
[60] C. Debbasch, S.B. De La Salle, F. Brignole, P. Rat, J.M. Warnet, C. Baudouin, Cytoprotective effects of hyaluronic acid and carbomer 934P in ocular surface epithelial cells, Invest. Ophthalmol. Vis. Sci. 43 (2002) 3409–3415.
[61] G. Abatangelo, R. Barbucci, P. Brun, S. Lamponi, Biocompatibility and enzymatic degradation studies on sulphated hyaluronic acid derivatives, Biomaterials 18 (1997) 1411–1415.
[62] K. Masuko, M. Murata, K. Yudoh, T. Kato, H. Nakamura, Anti-inflammatory effects of hyaluronan in arthritis therapy: not just for viscosity, Int. J. Gen. Med. 2 (2009) 77–81.
[63] A.C. Petrey, C.A. de la Motte, Hyaluronan, a crucial regulator of inflammation, Front. Immunol. 5 (2014), 101.
[64] J. Zhang, X. Xu, N.V. Rao, B. Argyle, L. McCoard, W.J. Rusho, T.P. Kennedy, G.D. Prestwich, G. Krueger, Novel sulfated polysaccharides disrupt cathelicidins, inhibit RAGE and reduce cutaneous inflammation in a mouse model of rosacea, PLoS One 6 (2011), e16658.
[65] M.S. Mulligan, M. Miyasaka, Y. Suzuki, H. Kawashima, M. Iizuka, A. Hasegawa, M. Kiso, R.L. Warner, P.A. Ward, T. Suzuki, Anti-inflammatory effects of sulfatides in selectin-dependent acute lung injury, Int. Immunol. 7 (1995) 1107–1113.
[66] G. Savini, P. Prabhawasat, T. Kojima, M. Grueterich, E. Espana, E. Goto, The challenge of dry eye diagnosis, Clin. Ophthalmol. 2 (2008) 31–55.
[67] I. Toda, J. Shimazaki, K. Tsubota, Dry eye with only decreased tear break-up time is sometimes associated with allergic conjunctivitis, Ophthalmology 102 (1995) 302–309.
[68] P. Daull, L. Feraille, P.P. Elena, J.S. Garrigue, Comparison of the anti-inflammatory effects of artificial tears in a rat model of corneal scraping, J. Ocul. Pharmacol. Therapeut. 32 (2016) 109–118.
[69] M.J. Doughty, Rose bengal staining as an assessment of ocular surface damage and recovery in dry eye disease-a review, Contact Lens Anterior Eye 36 (2013) 272–280.
[70] S.C. Pflugfelder, A. Solomon, M.E. Stern, The diagnosis and management of dry eye: a twenty-five-year review, Cornea 19 (2000) 644–649.
[71] R. Fu, Y. Jiang, J. Zhou, J. Zhang, Rebamipide ophthalmic solution modulates the ratio of T helper cell 17/regulatory T cells in dry eye disease mice, Mol. Med. Rep. 19 (2019) 4011–4018.
[72] B.J. Reiser, T.S. Ignacio, Y. Wang, M. Taban, J.M. Graff, P. Sweet, Z. Chen, R.S. Chuck, In vitro measurement of rabbit corneal epithelial thickness using ultrahigh resolution optical coherence tomography, Vet. Ophthalmol. 8 (2005) 85–88.
[73] S. Yeh, X.J. Song, W. Farley, D.Q. Li, M.E. Stern, S.C. Pflugfelder, Apoptosis of ocular surface cells in experimentally induced dry eye, Invest. Ophthalmol. Vis. Sci. 44 (2003) 124–129.
[74] C. Li, Y. Song, S. Luan, P. Wan, N. Li, J. Tang, Y. Han, C. Xiong, Z. Wang, Research on the stability of a rabbit dry eye model induced by topical application of the preservative benzalkonium chloride, PLoS One 7 (2012), e33688.
[75] W. Chen, X. Zhang, J. Li, Y. Wang, Q. Chen, C. Hou, Q. Garrett, Efficacy of osmoprotectants on prevention and treatment of murine dry eye, Invest. Ophthalmol. Vis. Sci. 54 (2013) 6287–6297.
[76] R. Sawazaki, T. Ishihara, S. Usui, E. Hayashi, K. Tahara, T. Hoshino, A. Higuchi, S. Nakamura, K. Tsubota, T. Mizushima, Diclofenac protects cultured human corneal epithelial cells against hyperosmolarity and ameliorates corneal surface damage in a rat model of dry eye, Invest. Ophthalmol. Vis. Sci. 55 (2014) 2547–2556.
[77] Q.C. Yang, J. Bao, C. Li, G. Tan, A.H. Wu, L. Ye, L.H. Ye, Q. Zhou, Y. Shao, A murine model of dry eye induced by topical administration of erlotinib eye drops, Int. J. Mol. Med. 41 (2018) 1427–1436.
[78] T. Kojima, M. Dogru, M. Kawashima, S. Nakamura, K. Tsubota, Advances in the diagnosis and treatment of dry eye, Prog. Retin. Eye Res. 78 (2020), 100842.
[79] L. Tang, X. Wang, J. Wu, S.M. Li, Z. Zhang, S. Wu, T. Su, Z. Lin, X. Chen, X. Liao, T. Bai, Y. Qiu, P.S. Reinach, W. Li, Y. Chen, Z. Liu, Sleep deprivation induces dry eye through inhibition of PPARα expression in corneal epithelium, Invest. Ophthalmol. Vis. Sci. 59 (2018) 5494–5508.